

UC Irvine

UC Irvine Electronic Theses and Dissertations

Title

Influence of size of the electrodes in detecting high frequency oscillations in human intracranial recordings

Permalink

<https://escholarship.org/uc/item/0j0673bb>

Author

Shamirian, Garineh

Publication Date

2019

Peer reviewed|Thesis/dissertation

**UNIVERSITY OF CALIFORNIA
IRVINE**

**Influence of size of the electrodes in detecting high frequency
oscillations in human intracranial recordings**

Thesis

Master's of Science
Biomedical Engineering

By
Garineh Shamirian

Thesis Committee:

Assistant Professor Beth Lopour, chair

Professor Frithjof Kruggel

Assistant Professor Daryl Preece

2019

Dedication

To my late parents

who throughout their lives etched in the walls of my heart the
importance of education.

Table of Contents

Dedication:	ii
Contents	iii
Table of Figures	iv
Table of Contents	v
Acknowledgments:	vi
Abstract of thesis:	vii
Chapter 1: Introduction	1
1.1 Motivation	1
1.2 Background on epilepsy treatment	3
1.3 Background on HFOs	4
1.4 Previous studies and their shortcomings	7
Chapter 2: Methods	11
2.1 Preliminary data and mathematical model	11
2.2 General experimental model	12
2.3 In vitro experiment	13
2.4 In vivo experiment	15
2.5 Preprocessing of the data	18
2.6 Automated detection	20
2.7 Simulated electrode configuration	23
2.8 Comparison of different configurations	24
Chapter 3 : Results	27
3.1 In vitro experimental analysis	27
3.2 Pre-processing of in vivo experimental data	29
3.3 Rate of detected HFOs	31
3.4 Statistical testing and comparison	36
Chapter 4 : Discussions and Conclusions	41
References:	45

List of Figures

Figure 1.1 . Electrophysiological measurements in epilepsy.	4
Figure 1.2. HFOs at three different spatial scales..	6
Figure 1.3. Amplitude of HFOs at different electrode size..	7
Figure 2.1 circuit model of electrodes and amplifier	11
Figure 2.2 Electrode configuration for in Vitro experiment	13
Figure 2.3 In Vitro experimental set up	14
Figure 2.4 Recording set up of the experiments	15
Figure 2.5 Electrode configuration for in vivo experiment	16
Figure 2.6 Example of junction box	17
Figure 2.7 Shorted electrodes with touch proof jumpers	18
Figure 2.8 Example of recorded raw data	20
Figure 2.9 The determination of threshold	22
Figure 2.10 Examples of automated detected HFOs	23
Figure 2.11 Flowchart of methods used	27
Figure 3.1 Peak to peak amplitude of electrodes in Vitro experiment	28
Figure 3.2 Shorted vs. unshorted signal in Vitro experiment	29
Figure 3.3 Power spectrum of two re-referencing in vivo experiment	31
Figure 3.4 SOZ marked by clinicians	32
Figure 3.5 Average rate of detected HFOs on a grid for ripple band	35
Figure 3.6 Average rate of detected HFOs on a grid for fast ripple band	36
Figure 3.7 Bar plot of sum of rates in each minute for ripple band	38
Figure 3.8 Bar plot of sum of rates in each minute for fast ripple band	39
Figure 4.1 Faraday cage diagram	44

List of Tables

Table 3.1 Percentage of detected HFOs in just one electrode.....	33
Table 3.2 Ranksum results for single vs. shorted pair.....	41
Table 3.3 Ranksum results for simulated pair vs. pair.....	41

Acknowledgments

First of all, I would like to express my sincere gratitude to my advisor, Prof. Beth Lopour. She generously offered her time, guidance, patience and good will through my graduate studies at UC Irvine. Her encouragement and support helped me through the challenges during my Master's study and research. She has been both an excellent mentor and a role model for me.

I wish to thank my committee members Prof. Frithjof Kruggel and Prof. Daryl Preece for their time to evaluate my work. Also, I sincerely enjoyed their lectures and appreciate what they taught me.

Also, I want to say thank you to Dr. Daniel Shrey at Children's Hospital of Orange County. He generously spared his time to help me with my data recording. He offered his insightful perspective as a clinician which was very helpful in my research.

Appreciations also go to all my lab members at lopourotoy, they always inspired me when facing obstacles and offered their generous help. Krit, who shared his experience with me generously.

And of course, I would like to thank my family for all their love and care. Special thanks to my husband for his help as a researcher in my study. Also, my brother who supported me during this journey.

Abstract of Thesis

Influence of size of the electrodes in detecting high frequency oscillations in
human intracranial recordings

By

Garineh Shamirian

Master of science in Biomedical Engineering

University of California, Irvine, 2019

Assistant Professor Beth Lopour, Chair

High frequency oscillations (HFOs) are promising biomarkers of epileptic tissue. However, the impact of the measuring electrode size on HFO detection remains unknown. We, therefore, proposed a novel experimental technique for detecting high frequency oscillations in human intracranial data, in which we dynamically changed the electrode sizes by electrically shorting them. This enabled us to record oscillatory activity from a single brain location using electrode sizes that range from 1.08 mm² to several square centimeters. This experiment was conducted in an in vitro modeling as well as an in vivo

experiment using ECoG grids. Shorting of the channels on the ECoG grid mimicked different surface areas for the contact electrodes. Our experimental study confirmed that the rate of the HFOs detected is impacted by the electrode size, with smaller electrodes detecting more events. The results of this experiment can help to have a better understanding of the underlying neural generators, also can be used to have more optimal recording parameters. The result can also be directly used in clinical practices for seizure onset zone localization and surgical planning.

Chapter 1: Introduction

1.1 Motivation

The term “neural oscillations” refers to the rhythmic and/or repetitive electrical activity generated in the central nervous system, based on Hans Berger’s (1873 - 1941) discovery, of the electroencephalogram (EEG). Normal cognitive processing in the brain is often associated with transient bursts in high frequencies. For example, high gamma band activity (80 - 150 Hz) is associated with memory [1], language perception and attention [2], and visual tasks [3]. Such high frequency brain oscillations have gained tremendous importance in recent decades, as they are physiological markers of a healthy brain and can also indicate brain abnormalities such as epilepsy [4, 5].

Epilepsy is one of the most common neurological disorders. Around ten percent of the world's population have experienced a seizure at least once in their lifetime. The third of this population will develop epilepsy [4]. In the United States alone, 2 million people are affected by epilepsy [6]. High frequency oscillations (HFOs) are a promising biomarker for epilepsy diagnosis, as they appear in many different epileptic syndromes and they can be detected with both intracranial and scalp electroencephalography (EEG), as well as magnetoencephalography (MEG)[6]. They have proven to be a powerful tool in detecting the seizure onset

zone (SOZ)[6]. The surgical removal of brain regions exhibiting higher rates of HFOs is correlated with seizure freedom or significant reduction in seizure frequency [6 9]. This gives HFOs the great potential for clinical use in epilepsy diagnosis and treatment management.

In spite of these promising results, HFOs are not currently used in routine clinical and surgical planning. One reason for this is that the fundamental characteristics of HFOs remain unknown. Different sizes of electrodes, from 50 μm invasive microwire electrodes to scalp electrodes with 1 cm diameter, are used in neurological recordings for epilepsy. Currently, no distinction is made for HFOs measured at these different spatial resolutions. However, it is unlikely that all oscillations measured across this broad spatial resolution represent the same physiological events. Therefore, further studies are essential to understand these differences to use HFOs for diagnosis and treatment purposes for epilepsy, as well as to uncover their characteristics in a healthy brain. High localized HFOs detected by a micro electrode and not the adjacent one is likely to be generated with a different mechanism than the events detected by larger scalp EEG electrodes. The size of the underlying neural generators in seizures remains unclear. Quantification of the spatial properties of HFOs could reveal information about the size of the underlying neural generators. A better understanding of spatial properties of HFOs can improve diagnosis and clinical management of epilepsy, which would impact the lives of 65 million people worldwide suffering from this disease.

1.2 Background on epilepsy treatment

Clinical diagnosis of epilepsy relies on visual analysis of EEG recordings, in combination with the patient's medical history, laboratory testing, neurophysiological data, and brain imaging.

The standard treatment for epilepsy consists of one or more anti-seizure medications. In cases where medication is insufficient to prevent seizures, surgical treatment may be considered. The purpose of resective surgery is to remove the part of the brain causing the seizures, ideally leading to seizure freedom or a significant reduction in seizure frequency in the patient.

During the pre-surgical procedure, clinicians aim to localize the brain regions where the seizures originate from, termed the seizure onset zone (SOZ). EEG has poor spatial resolution, so in order to localize the SOZ with better accuracy, patients have intracranial electrodes surgically implanted in and on the surface of the brain regions with a high likelihood of being in the SOZ. Then spontaneous electrophysiological data is directly recorded until several seizures are captured. The electrode(s) at which seizure activity is first detected are marked as the SOZ and are typically the target area for the surgery.

Different types of intracranial electrodes are used in this procedure. Examples are electrocorticogram (ECoG) grids or strips on the cortical surface or depth or stereotactic EEG electrodes that pierce into the tissue and target deeper brain structures (Figure 1.1).

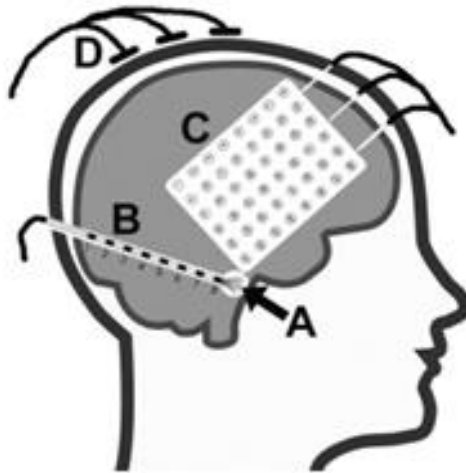


Figure 1.1. Electrophysiological measurements in epilepsy. (A) Microelectrode wires, 40 μm diameter. (B) 8-channel stereotactic EEG, electrode contact area 0.8 mm^2 . (C) 6x8 ECoG grid, electrode contact area 4-5 mm^2 . (D) Scalp EEG contact area $\sim 50 \text{mm}^2$. (A)-(C) are invasive measurements, requiring surgery.

1.3 Background on HFOs

Studies of neural oscillations have revealed oscillatory activities are in specific frequency bands that characterizes them [10]. These oscillations are typically categorized into five frequency bands: delta (0.5-4Hz), theta (4- 8Hz), alpha (8-13Hz), beta (13-30Hz) and gamma (>30Hz) [10]. In addition to these widely studied bands, in recent years there has been a rising interest in studying brain oscillations at higher frequencies, HFOs. As they are correlated with pathological brain activity [11].

While current clinical practice relies on directly recording a patient's seizure, HFOs are investigated to be potential biomarkers for epileptogenic brain tissue [12]. They are directly linked to the SOZ; electrodes in the SOZ typically

exhibit higher rates of HFOs than electrodes outside the SOZ. Therefore, can be used as potential target of surgery [13, 14- 16]. Respectively, resection of brain areas identified as generating pathological HFOs leads to improved postsurgical outcomes in patients with refractory epilepsy [12, 14, 16-18].

HFOs are field potentials that reflect short-term synchronization of neural activity (normally lasting less than 100ms) and they occur more frequently during non-rapid eye movement (NREM) sleep. Based on visual observation, HFOs are described as spontaneous events of at least 3-4 consecutive oscillations that stand out from the background activity. [2]. The frequency range for HFOs is typically divided into two groups, ripple band (RB) (80 - 250 Hz) and fast ripple band (FRB) (250 - 500 Hz) [13]. HFOs have been detected with a wide range of electrode sizes in neural recordings, including microwires [7], stereotactic EEG [19], depth electrodes and ECoG grids [20-22], and scalp EEG electrodes [23- 24]. (Figure 1.2). HFOs believed to play a crucial role in both normal and pathological brain activity [11]. They are associated with a wide variety of epilepsies, such as temporal lobe epilepsy [6], neocortical epilepsy [25], infantile spasms [26], and tuberous sclerosis [27].

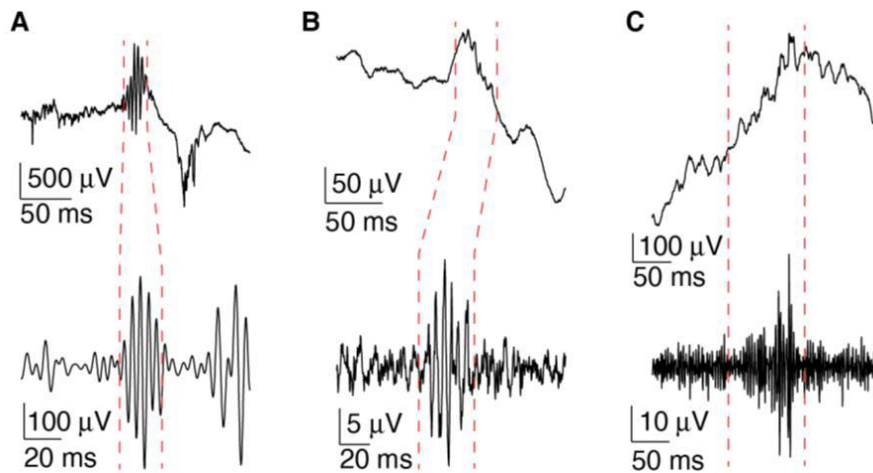


Figure 1.2. HFOs (between red dashed lines) at three different spatial scales. Broadband data is shown in the top row, and the bottom row shows the signal after filtering in the frequency band of interest. (A) Ripple in microelectrode data. (B) Ripple in depth electrode data. (C) Fast ripple in scalp electrode data. Data was recorded at UCLA (A, C) and UCI (B).

Theoretically, the size of the HFO neural generator, which is proportional to the number of contributing neurons, is related to the amplitude of the measured electrical potentials [28]. There is an almost linear relationship between the amplitude of the measured electric potential and the extent of the generator in the cortex [28]. Simultaneous recordings of microelectrodes and macroelectrodes suggested that larger electrodes are advantageous for detecting ripple band oscillations [29], while small electrodes are superior for fast ripple detection [15]. However, a meta-analysis performed on published data from twelve independent studies showed that there is no decrease in the amplitude of detected HFOs as the electrode's surface area increases (Figure 1.3) [3, 13, 17, 19, 24, ,30- 36]. In theory, the amplitude should be a function of electrode size.

However, figure 1.3 demonstrates there is no decrease in the amplitude as the electrode size increases.

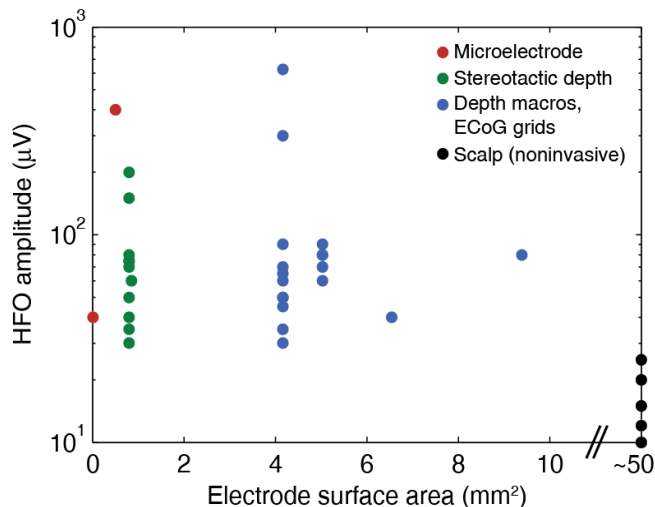


Figure 1.3. When recorded with intracranial electrodes, the HFO amplitude is not correlated to electrode surface area. Data are aggregated from 12 independent studies with different electrode types (indicated by color) and recording locations.

1.4 Previous studies and their shortcomings

Previous studies have suggested that the size of HFO generators (and especially fast ripple band generators) are less than 1 mm³ [37], suggesting that smaller electrodes will have an advantage in detecting them. Furthermore, a study by Worrell et al. compared the HFO detection rates with different contact sizes [15]. This study demonstrated a significant advantage in using smaller electrodes for HFO detection, such as microwires, as opposed to larger, clinical depth electrodes [37]. Specifically, the rate of HFOs detected by clinical depth electrodes with a surface area of 9.4 mm² was compared to the rate detected by

microwires with surface area more than 7000 times smaller (wire diameter of 40 μm , surface area of 0.0012 mm^2). Worrell et al. report was based on simultaneous recordings of HFOs using specifically designed hybrid electrodes containing both micro and macro contacts in seven patients with mesial temporal lobe epilepsy [37]. To detect the HFOs, an automated detection tool was used with further visual verification. 74% of detected HFOs were recorded on a single electrode and were not visible on the adjacent microcontacts (with 1 mm distance) or macrocontacts (2-5 mm distance). Overall, only 33% of ripple band HFOs and 19% of fast ripple band HFOs were detected in macro electrodes. This large difference in the rate of detected HFOs signifies the importance of the size of contacts used in HFO recordings. These findings are consistent with previous hypotheses that HFOs are very localized events [29]. Theoretically, smaller electrodes would record activities both generated by more localized neural generators as well as large neural generators by single electrodes, whereas larger electrode contacts would detect only events generated by a larger neural volume. While larger electrodes cannot detect events with small neural generators, they may still record a large number of events because they sample from a large volume of tissue [29].

In addition, Zelman *et al.* simultaneously recorded EEG and ECoG and found that only 38% of scalp HFOs could be predicted from their ECoG counterpart using a linear model [34]. This suggested a complex relationship between the generator size and HFO amplitude. However, in this experiment the

comparison relied on different electrode types, and the data was aggregated from different patients and recording locations.

Another study done by Chatillon et al. on epileptic rats, examined rate of occurrence, mean spectral frequency, amplitude, and duration of hippocampal HFOs in relation to surface area of the contacts [29]. Electrodes with three different sizes (0.018, 0.051, and 0.85 mm²) were used for HFO detection. In their analysis, they found no significant difference in the rates of occurrence or other aspects of HFOs with respect to the electrode size. However, based on a review paper by Prida et al. where the impact of electrode size in HFO detection was analyzed based on different studies, the rates were higher in Chatillon et al. study compared to studies reported before such using smaller electrodes [38]. The higher rates in this study can be associated with large electrodes. Since, larger electrodes sample from a larger area than can potentially contain more HFO generating sites. If this assumption is correct, then it is unclear why the former study was unable to detect any differences.

The review paper by Prida et al. also provided recommendation on the size of the electrodes to obtain comparable HFOs signals in clinical and basic research in epilepsy [38]. In this review, unsolved questions about epilepsy was discussed, including the role of electrode sizes. It appeared that the advantage of using macroelectrodes is their capability to sample larger areas. Therefore, potentially recording multiple HFO sites. In this case as the electrodes are spaced farther apart from one another, as the result in the recordings uncorrelated HFOs were spatially averaged together and interfering signals are included.

Therefore, the measured HFO does not be used to accurately localize the activity site. On the other hand, microelectrodes provide better spatial resolution, but in cases where the HFO generating sites are small and scattered, then this will require precise placement of microelectrodes to capture maximum possible active regions. In general, in this review, high density microelectrode arrays were suggested in the human epileptic brain measurements to better understand mechanisms generating normal and pathological HFOs [38].

We used a novel recording technique that allowed us to dynamically change the electrode size, and importantly, this technique is compatible with standard clinical procedures. As suggested by previous studies we used high density mini grid to measure human intracranial data with electrode sizes ranging from 1mm^2 to several square centimeters. We hypothesized that the rate of detected HFOs will vary based on the size of the electrode used in recording.

Chapter 2: Methods

2.1 Preliminary data and mathematical model

A lumped electrical circuit model of the electrode-brain interface can provide a testable hypothesis for the relationship between electrode size and HFO amplitude (Figure 2.1A)[39, 40].

We begin by modeling two cortical surface electrodes (with impedances Z_{e1} , Z_{e2}) that are each connected to an amplifier (with impedances Z_{a1} , Z_{a2}) (Figure 2.1B). The electrodes sense independent voltage sources in the neural tissue (V_{s1} , V_{s2}), which interact through the impedance of the tissue itself (Z_{b1} , Z_{b2} , Z_{12}). We can then derive a relationship between the electrical potential at the brain/electrode interface (V_{b1}) and the two voltage sources: $V_{b1} = \frac{Z_{b2} + Z_{12}}{Z_{b1} + Z_{b2} + Z_{12}} V_{s1} +$

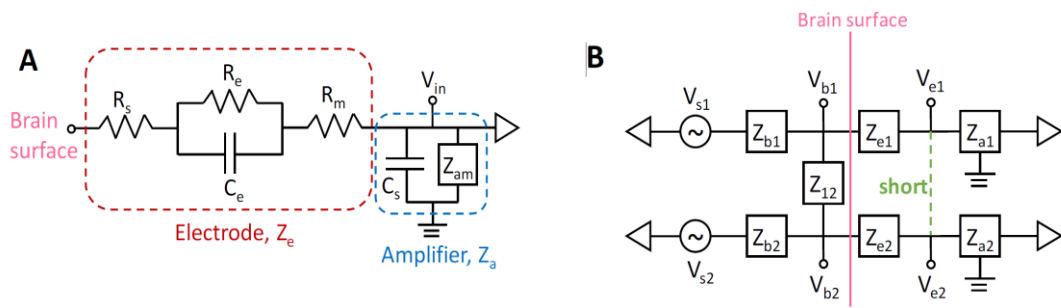


Figure 2.1: (A) Circuit model of a single electrode (red box) connected to an ideal amplifier (blue box). (B) Circuit model of two electrodes (Z_{e1} , Z_{e2}) on the surface of the brain that can be shorted together (green dashed line) to simulate an electrode with twice the surface area.

$\frac{Z_{b1}}{Z_{b1}+Z_{b2}+Z_{12}}V_{s2}$. Assuming $Z_{b1} \approx Z_{b2} \approx Z_{12}$, we find that the voltage at each electrode is $V_{e1} = \frac{2}{3}V_{s1} + \frac{1}{3}V_{s2}$ and $V_{e2} = \frac{1}{3}V_{s1} + \frac{2}{3}V_{s2}$.

To represent an electrode with twice the surface area, we model two adjacent electrodes that are shorted together (Figure 2.1B, green dashed line). Then the common signal ($V_{e1}=V_{e2}=V_e$) that would be sensed at the input to the amplifier is $V_{b1} = \frac{Z_{e2}}{Z_{e1}+Z_{e2}}V_{b1} + \frac{Z_{e1}}{Z_{e1}+Z_{e2}}V_{b2}$, where $V_{b1} = \frac{z_{b2}(z_e + z_{12}) + z_{12}z_e}{(z_e + z_{12})(z_{b1}+z_{b2}) + z_{12}z_e}V_{s1} + \frac{z_{b1}(z_e + z_{12})}{(z_e + z_{12})(z_{b1}+z_{b2}) + z_{12}z_e}V_{s2}$ and V_{b2} is analogously defined. Therefore, when two electrodes are shorted together, the voltage measured by the amplifiers is a linear combination of the voltages sensed by each individual electrode (V_{b1} and V_{b1}). Further, if we assume approximately equal electrode impedances, we find that V_e is the average of the two voltages: $V_e = \frac{1}{2}(V_{b1} + V_{b2})$. In the likely scenario that the signal generators are correlated, but not perfectly equal, e.g. $V_{s1} = V$ and $V_{s2} = 0.5V$, we find that $V_e = \frac{3}{4}V$, which is smaller than $\max\{V_{e1}, V_{e2}\} = \frac{5}{6}V$. Therefore, increasing the electrode size should lead to a decrease in HFO amplitude, contrary to reported data (Figure 1.3).

2.2 General experimental model

We tested this hypothesis using a 20 channel EcoG grid through an in vitro as well as in vivo experimental models. We electronically shorted adjacent electrodes by physically connecting them together to simulate different electrode

surface areas. We tested single electrodes, adjacent pair shorted electrodes and four connected (2x2) electrodes as different electrode configurations (Figure 2.2). These different configurations each mimicked a different electrode surface area.

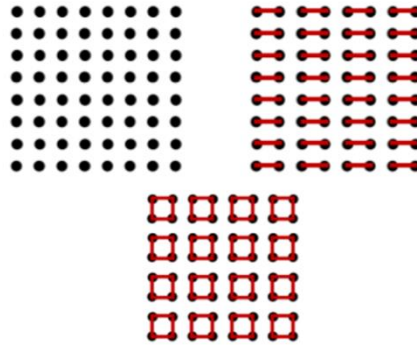


Figure 2.2: Electrode configurations. Black dots are electrodes and red lines indicate a short between electrodes. The three different electrode sizes.

2.3 In vitro experiment

The theoretical basis of our hypothesis was first tested by an in vitro experiment. In the in vitro experiment, agar gel was used as the phantom brain tissue. Agar is a common substitute for brain tissue, as it has been shown to mimic both physical [36] and electrical properties of the human brain, including impedance [41] and conductivity [37]. The gel weight was 1.2%, mixed with water and NaCl with concentration of 1.0 mg/ml to provide conductivity similar to brain tissue (~ 0.33 S/m) [39]. A 4x5 electrode EcoG grid was used for this part of the experiment. Only 16 electrodes were used in the measurement

The 4x5 EcoG grid was placed on the surface of the agar gel and two wires electrodes was implanted within the gel for bipolar stimulation (Figure 2.3).

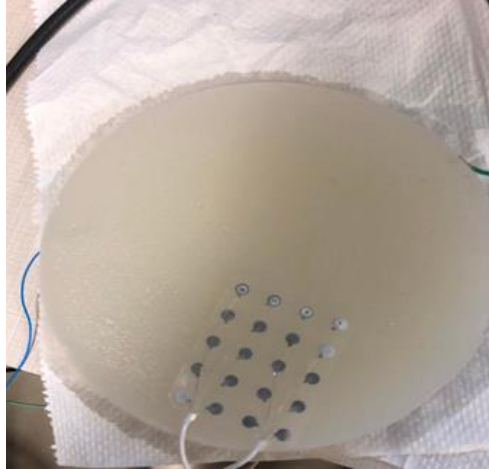


Figure 2.3: Experimental set up with mini grad placed on the agar gel.

The wire electrode was connected to an electrical signal generator to provide sinusoidal electrical stimulation, as representative of an HFO source. Simultaneously, measurements were recorded through the 4x5 EcoG grid electrodes. Then, as shown in Figure 2.2, adjacent electrodes were shorted together to create electrodes with larger surface areas. Measurements were repeated for each electrode configuration. The 4x5 EcoG grid electrodes have an exposed surface area of 5 mm^2 with 1 cm spacing; consequently, as two adjacent electrodes are paired together the surface area is increased to 1.5 cm^2 , an eight electrode grid is simulated with a surface area of 4 cm^2 for each electrode.

In the next step, four electrodes were connected, i.e. 2×2 blocks of electrodes were shorted together to create four electrodes, each with surface area of 4.18 mm^2 . The electrodes were connected to a junction box and an EEG

amplifier. The data were sampled at a rate of 4000 Hz by a PC. Electrodes were shorted together before entering the amplifier using touch proof jumpers (Figure 2.4). All electrodes were referenced to a grounded electrode on the surface of the gel

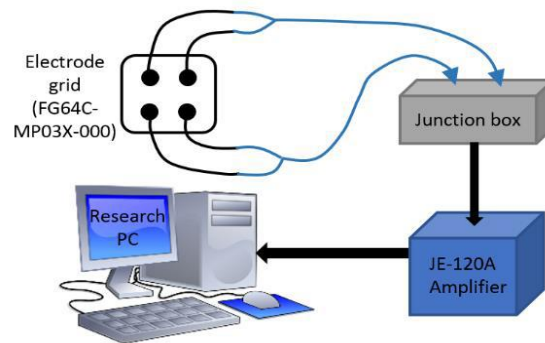


Figure 2.4. Recording setup, showing acquisition hardware for the in vitro and in vivo studies. Here

The resulting measurements were compared to the electrical circuit model predictions. We expected that the bipolar electrical stimulation would create a dipole electric field in the measuring 4x5 ECoG grid. Also, we expected the amplitude of the sinusoidal signal to decrease as the electrode surface area increased.

2.4 In vivo experiment

We designed a similar in vivo experiment based on the theoretical method, with the goal of recording HFOs with electrodes of different sizes.

Data for this experiment was recorded from a patient diagnosed with epilepsy who was already undergoing intracranial electrode monitoring in preparation for surgery. Data was recorded at the Children's Hospital of Orange County (CHOC), in collaboration with epileptologist Daniel Shrey, MD and neurosurgeon Joffre Olaya, MD. Approval for this study was obtained from the Institutional Review Board of the Children's Hospital of Orange County (CHOC). Parental consent and, when appropriate, pediatric assent, were obtained prior to study enrollment. An 8x8 (Ad-Tech FG64C-MP03X-000) High density (HD) ECoG grid (with electrode surface area size of 1.09 mm² with center to center spacing of 3 mm) was implanted on the brain region that was hypothesized to be associated with seizure onset zone based on prior clinical diagnosis. This placement was assumed to maximize the possibility of recording HFOs. Note the electrodes used in this experiment were already FDA approved for human use.

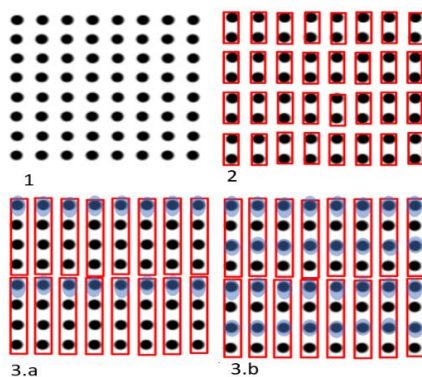


Figure 2.5: Electrode configuration for in vivo post- surgical recording. Black dots represent the electrodes. Red boxes indicate the shorted electrodes together 1. Single electrode. 2. Paired electrodes. 3.a. Quad electrodes, recording is only from one electrode (blue). 3.b. Quad electrodes with recordings of two electrodes (blue).

During the post-surgical monitoring period, while clinicians waited for the seizure to occur, we recorded four electrode configurations (Figure 2.5) for 18 - 24 minutes for each configuration, while referencing to one corner electrode of the grid. This amount of time was assumed to be sufficient to capture around 100 HFOs or more. Data was recorded at awake and asleep state of the patient. However, due to noise complications only asleep state data was used for analysis. Similar to figure 2.4 illustrations, shorting of electrodes were done using touch proof wires before entering the junction box (T- connector). Input of the T-connector are wires of each channel of the electrode grid (Figure 2.6).

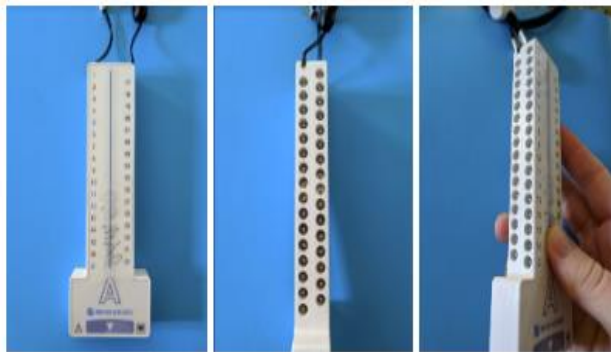


Figure 2.6: Example of junction box - T - connector. Electrode wires are the input.

Touch proof jumpers connect the input electrodes of a specific configuration that will electronically short the electrodes and simulate different contact surface area (Figure 2.7). Based on the mentioned electrode configurations (Figure 2.5), surface areas of 1.17 mm^2 for single electrodes, 5.34 mm^2 for shorted pair electrodes and 13.68 mm^2 for quad configuration was achieved. The recorded data was sampled at the rate of 5000 Hz by a PC.



Figure 2.7: Touch proof jumpers are used to short/ connect the

2.5 Preprocessing of the data

In the pre-processing stage, two different referencing montages, common average and bipolar, were applied to the data. In common average referencing, the average across all channels for each time point was calculated and subtracted from the value of each sampled data of the corresponding channel. This method will provide a common reference for all channels. This method is preferred because each channel will contain data from a single electrode, making it easier to compare the single, pair, and quad configurations. In bipolar referencing, the value for each electrode is referenced to (subtracted from) the electrode adjacent to it. This is done for each column of 8 channels, so after bipolar referencing, the measurement from a 64-electrode grid is represented as

56 channels. Despite the advantages of common average referencing, a bipolar montage was adopted as the re-referencing technique for this study because it was more efficient in eliminating noise. The interface displaying the raw data for a 90-second segment with bipolar referencing is shown in Figure 2.8.

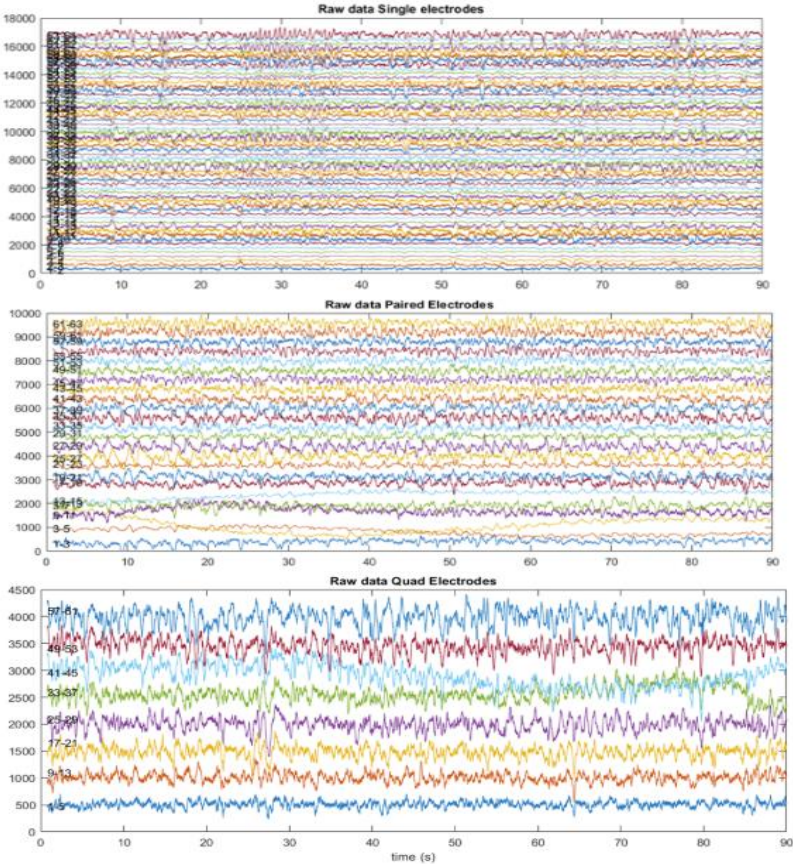


Figure 2.8: Raw data examples for 90 seconds of data. Top: Single electrodes. Middle: Paired electrodes. Bottom : Quad electrodes.

Data was then segmented into one minute windows for our analysis. Two bandpass filters were applied to isolate ripple band and fast ripple band

frequencies. For the ripple band, we used a bandpass filter with passing range 80 - 250 Hz (least-square linear phase finite impulse response filter, $f_{stop1} = 70$ Hz; $f_{pass1} = 80$ Hz; $f_{pass2} = 250$ Hz; $f_{stop2} = 260$ Hz; stopband attenuation = -80 dB), and for the fast ripple band we used a bandpass with passing frequencies 250 - 500 Hz (least-square linear phase finite impulse response filter, $f_{stop1} = 240$ Hz; $f_{pass1} = 250$ Hz; $f_{pass2} = 500$ Hz; $f_{stop2} = 510$ Hz; stopband attenuation = -80 dB). The signals were filtered forward and backward to obtain zero phase difference.

2.6 Automated detection

An automated detector, first published by Chapuranit et al., was used to detect HFOs [42]. In the automated detection algorithm, the bandpass filtered data was rectified and each “peak” (local maximum) in the rectified data was identified and measured as the amplitude of each oscillatory cycle. Events in which a number of consecutive peaks exceeded a threshold were marked as HFOs. In this automated procedure, instead of visually setting the threshold value, an iterative process was designed to determine the threshold based on the amplitude distribution of the signal. Therefore, only one parameter, α , indicating the tolerance for false positives was used. A higher α value will result in a lower threshold and the inclusion of more peaks.

In the algorithm designed by Chapuranit et al. in the iterative process of determining the threshold, a gamma distribution $f(x)$ was fit to the amplitude distribution of the rectified data, representing the amplitudes of the background activity in our data. We then calculated the cumulative distribution function $F(x)$ based on the distribution function $f(x)$. A cut off value of $F(x) = 1 - \alpha$ was defined, and all peaks with values above the cut off were excluded from the distribution. The fitting and exclusion of peaks was repeated for the new distribution until no more peaks were excluded. The final cutoff value was used to set the threshold [42] (Figure 2.9).

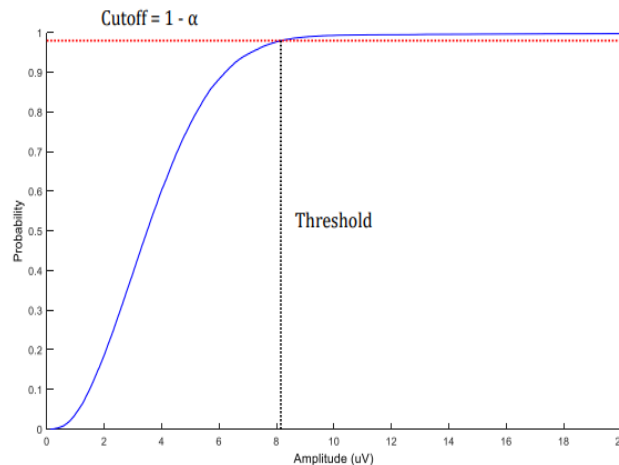


Figure 2.9: The determination of threshold. The threshold was determined using cutoff value $1 - \alpha$, which is based on the cumulative distribution function (blue line) of the peak amplitude.

After the threshold was set, if 5 out of 6 consecutive local maxima (peaks) in the rectified data were above the threshold, that event was labeled as a detected HFO. The detection was applied to both the ripple band and the fast

ripple band separately for three different α values, 0.02, 0.03 and 0.05. Figure 2.10 shows examples of detected HFOs.

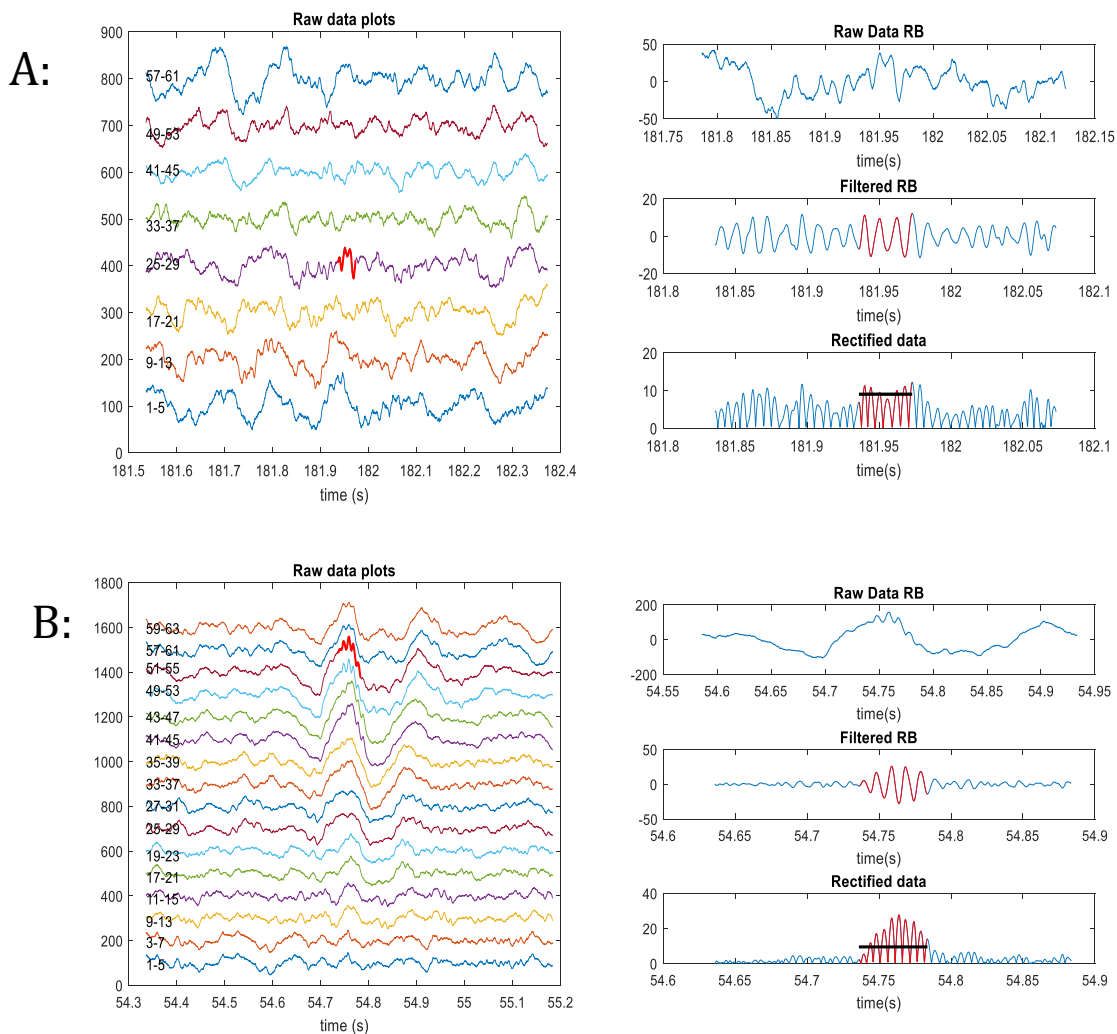


Figure 2.10: Examples of automated detected HFOs. In both A and B, the left figure shows the raw data in all channels with the detected HFO in bold red. On the right top is the raw data of the channel with the HFO. In the middle is the filtered data for the ripple band, and the bottom is the rectified data with the black line indicating the threshold for the detection. A is for the quad configuration with $\alpha = 0.05$. B is for the paired electrode configuration with $\alpha = 0.02$.

After detection, visual verification of the detected HFOs revealed many false positive detections for the quad configuration due to the presence of excessive noise in this electrode configuration. Therefore, data from this configuration was excluded from further analysis. For the single and paired data, random HFOs were selected, and the rectified data for the detected event was compared to the raw data. We noted some false positives due to noise oscillations around the zero-line. As we mainly relied on the performance of the auto detector. we did not address this through further post-processing.

2.7 Simulated electrode configuration

To compare the theoretical model of mathematical averaging of electrodes to the results from physically shorting adjacent electrodes, we simulated a paired electrode model from the single electrode data. In the simulated data, the paired electrode configuration is replicated by averaging the data of the two single electrodes that were shorted together in the paired configuration. Then the same steps of bipolar referencing, filtering and automated HFO detection with three different α values were applied to the simulated data, and finally, the rate of detected HFOs was calculated.

2.8 Comparison of different configurations

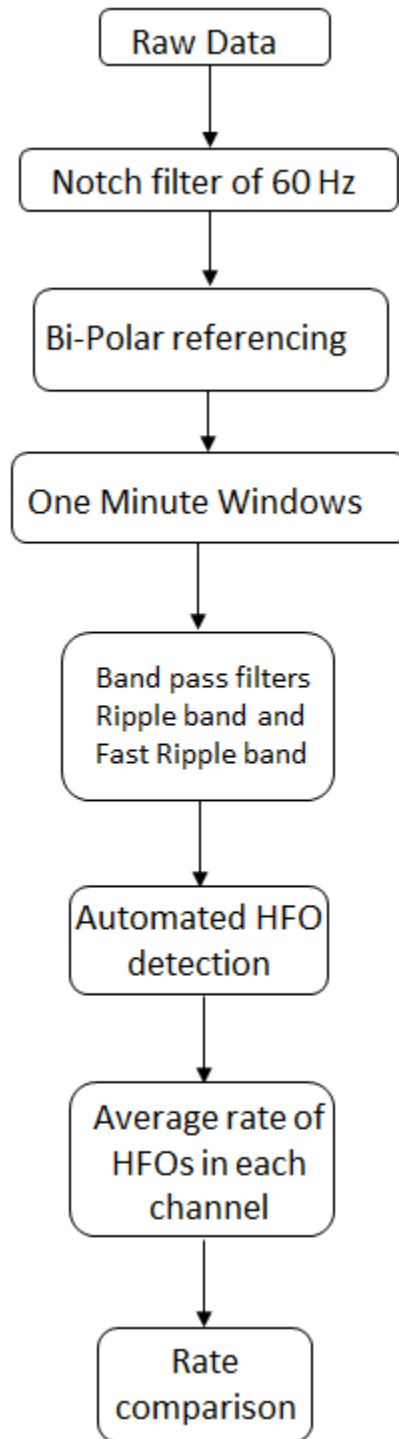
To investigate the influence of the contact size in detecting HFOs, we compared the rates of detected HFOs in different electrode configurations. For large events, where the region of brain tissue generating the HFO is larger than one electrode, the same HFO event might have been detected by more than one electrode. In order to avoid duplicate counting, we identified overlapping HFOs detected simultaneously in two or more channels. Specifically, HFOs detected in different channels that overlapped by 50 ms or more were considered to be the same event and were counted only once. Considering the complex, folded nature of the cerebral cortex, spatial layout restrictions on detecting overlapping events was unfeasible. Therefore, in this analysis, the overlap in time was the only determining factor used.

After overlap exclusion, a non-parametric statistical comparison test, the Mann-Whitney U test, or Wilcoxon rank sum test, was used to compare the HFO rates for different electrode configurations, hence different contact sizes. This tests the null hypothesis that the rates of HFOs in two different electrode configurations are samples from distributions with equal medians, against the alternative that the rates of detected HFOs are indeed different for each configuration.

Two comparisons were repeated for all three α values: single against shorted paired and simulated paired against shorted paired. In each case, the total rate of detected HFOs in each minute was calculated by adding the

individual rates for all channels, while counting the overlapping events only once. We then used the ranksum function in MATLAB to test the difference between distributions for two electrode configurations (where each element in the distribution represented the total rate in each minute for that configuration).

This test gives us the means to verify our hypotheses. First, the rank sum test performed on single versus shorted pair electrodes signifies the influence of electrode size on the rate of HFO detections. Second, the results of the rank sum test on simulated pair versus shorted pair demonstrates the difference between theoretical mathematical averaging and physical contact size.



Flowchart 2.11:
Flowchart of methods used in our analysis.

Chapter 3 : Results

3.1 In vitro experimental analysis

For the in vitro (gel) experiment, we compared the peak to peak values of the signal amplitudes measured by all electrodes for the three different electrode configurations (Figure 3.1).

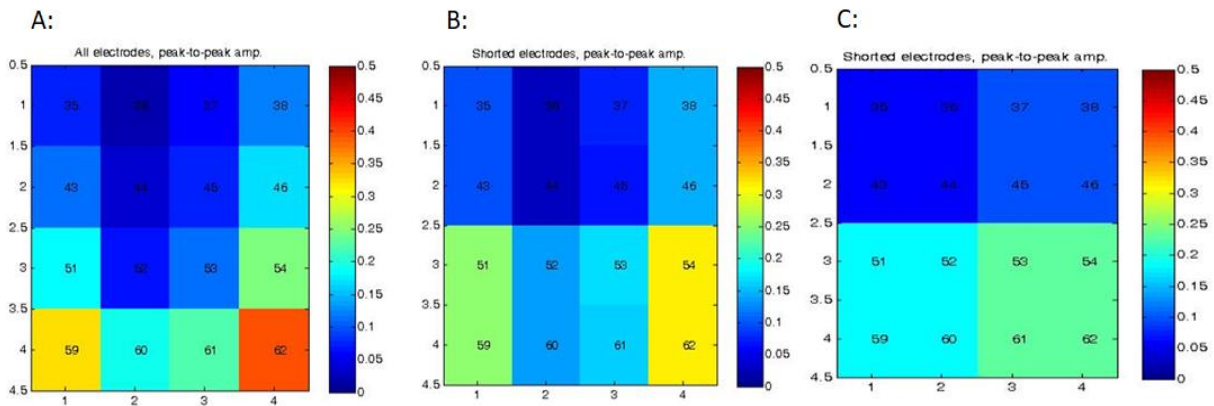


Figure 3.1: Peak to peak amplitude for different electrode configurations on the grid. A : unshorted - single electrodes, B : Shorted paired electrodes. C : Shorted 2x2 electrodes

The electrode closest to the source of the simulation (bottom right corner, electrode number 62) exhibited the highest amplitude signal. The amplitudes in the other electrodes follow the dipole pattern created by the electric field of the source simulator.

Figure 3.2 shows signals recorded from single electrodes (black) overlaid by the signals recorded from shorted electrodes (red). The shorted electrode configuration reported approximately - but not exactly - the average of single

electrode signals. This suggests that size of the electrode significantly affects the amplitude. The results also show, in contrast to previous assumptions, that in some channels, the amplitude does decrease (and in other channels, the amplitude increases). For an HFO, which will probably be the largest signal around, this averaging is likely to decrease its amplitude. as the surface area of the electrodes increased, which is consistent with the theoretical model of volumetric averaging.

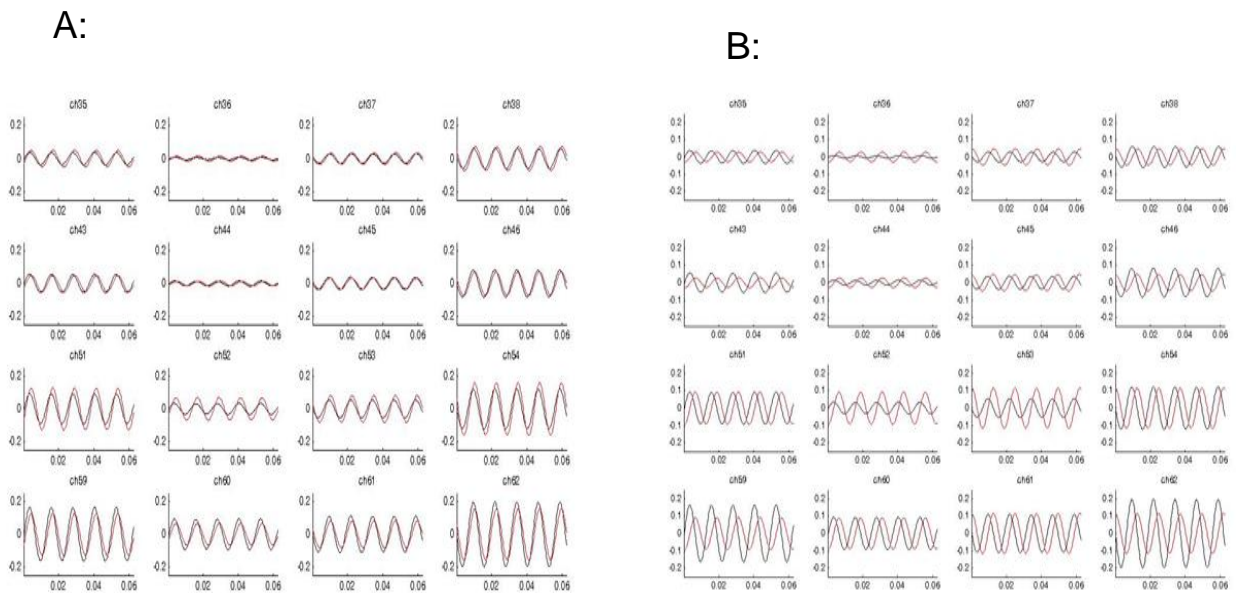


Figure 3.2: Black is for unshorted (single) electrodes and red is for shorted electrodes. A : Single electrode and Paired electrodes. B : Single electrode and 2x2 shorted electrodes.

3.2 Pre-processing of in vivo experimental data

In pre-analysis of our in vivo experimental data, we noted excessive line noise in the recordings, especially in the quad configuration. The jumpers used to short the electrodes together are likely the cause of the noise; we needed to use 48 jumpers to create the quad configuration, and each one can act as a small antenna. We applied two different re-referencing schemes to the data to reduce the noise. The preferred technique was a common average reference. However, the power spectrum of our data in each configuration suggests that bipolar re-referencing is more successful in reducing the excessive line noise (Figure 3.3). Note that, in the power spectrum of the quad electrode configuration, 60 Hz and the harmonics of line noise are present for both re-referencing techniques. Therefore, recordings from this configuration were not further analyzed in this study. Potential solutions to this problem, for future studies, will be described in the Discussion section.

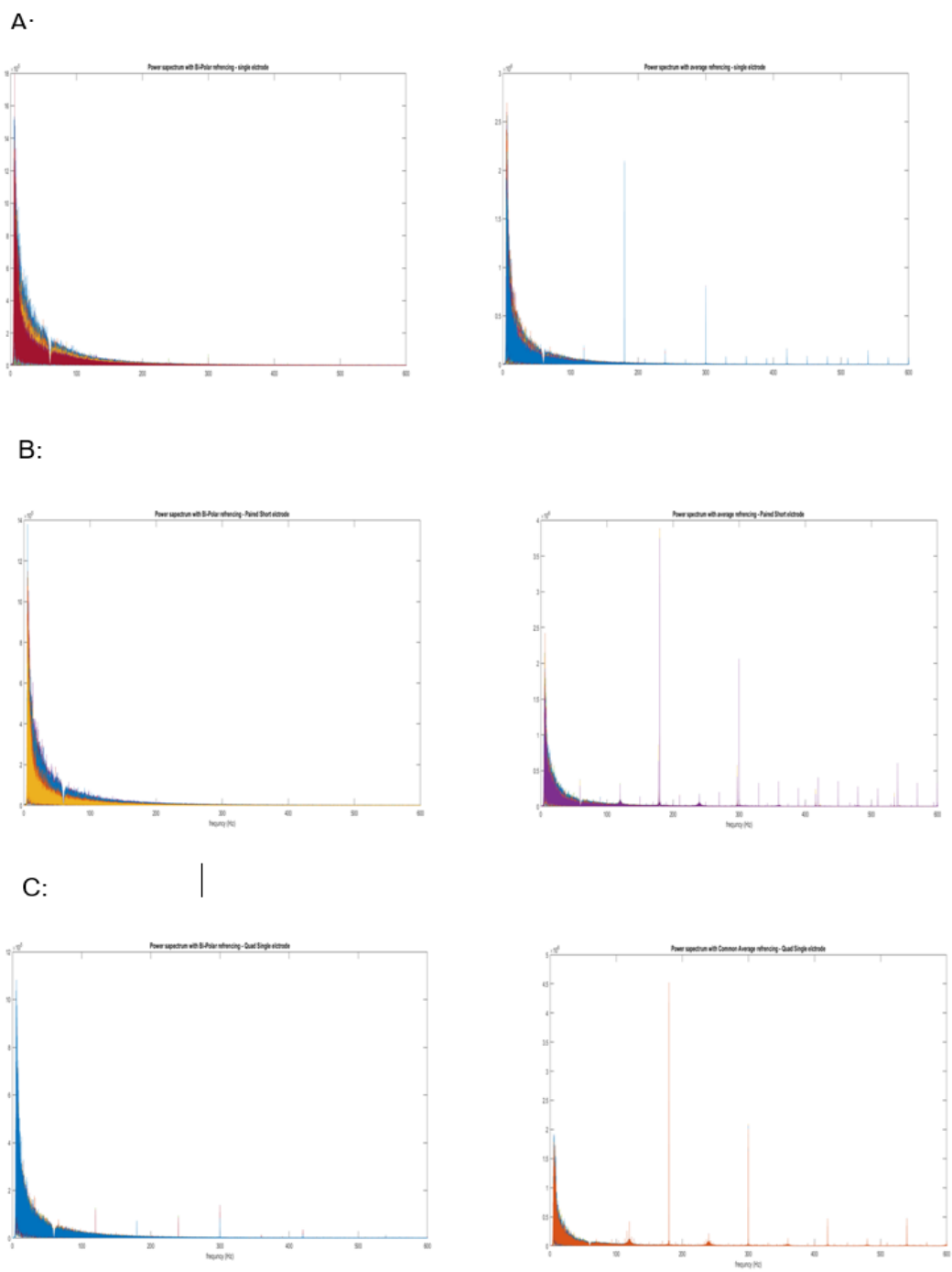


Figure 3.3: Power spectrum with two re-referencing mechanisms. A: single electrode. B: Paired electrodes. C: Quad electrodes. The left column shows bipolar referencing and the right column shows common average referencing. The bipolar referencing successfully removed the noise in the single and paired configurations. It reduced the noise for the quad configuration, but some peaks at 60 Hz harmonics are still visible.

3.3 Rate of detected HFOs

First, we compared the spatial pattern of HFO rate in each channel of the HD ECoG grid to the location of the SOZ identified by clinicians (Figure 3.4). Determination of the SOZ was based on evaluations of scalp EEG during multiple seizures, together with the patient's, brain imaging, and the patient's medical history.

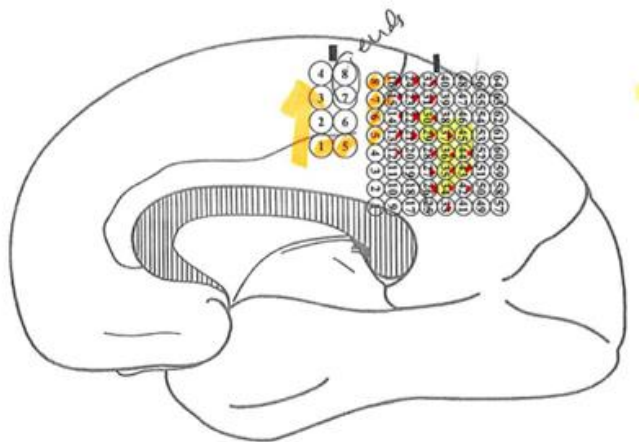


Figure 3.4: SOZ determined by clinicians. On the minigrd, the seizure starts in the electrodes marked in light yellow (electrodes 29, 20, 34-37, 43-45). Electrodes marked in red are involved in the subsequent build up and spread of the seizure.

HFO rates in the ripple band (Figure 3.5) did not appear to be correlated to the SOZ, but HFO rates in the fast ripple band (Figure 3.6) were highest in the SOZ electrodes. This is consistent with many previous studies suggesting a correlation between the location of fast ripples and the SOZ. Note that, in this part of the analysis, we did not exclude overlapping HFOs. Doing so would have

required us to arbitrarily assign each event to a single electrode, which would have altered the spatial distribution of events.

As mentioned before, higher α values result in a lower threshold for HFO detection in the automated detection algorithm. Consistent with this, as shown in Figures 3.3 and 3.4, the higher α values resulted in higher rates of HFOs. Also, in the contrary to previous studies, the rate of detected HFOs is higher in fast ripple band than in ripple band, as expected. In the ripple band for all α values, electrodes 21 and 22 have very high HFO rates. Further analysis in these channels verified detection of real HFOs. Even though, this channel was not labeled as SOZ. .

In both the ripple and fast ripple bands, the HFO rate decreased as the surface area of the electrode increased (Figures 3.5 and 3.6). Smaller electrodes likely detected events generated by more localized neural sources that were not visible to larger electrodes. The number of total detected HFOs with eliminating overlapping HFOs are compared to total number of HFOs without excluding the overlaps in single configuration to demonstrate this difference. Table 3.1 show the results of what percent of HFOs were detected only by one electrode.

α value	0.02	0.03	0.05
Ripple band	57.7%	36.1%	41.8%
Fast Ripple band	13.9%	11.1%	32.6%

Table 3.1 : Percentage of detected HFOs by only one electrode compared to all detected HFOs in single electrode configuration

The spatial pattern of HFO rate was similar for the simulated paired electrodes and the physically shorted electrodes (compare the middle and right-hand columns in Figures 3.3 and 3.4). However, the simulated data had slightly higher rate in detections, suggests that some HFOs are not captured by paired electrodes. Having access to data with quad configuration would make this demonstration more robust.

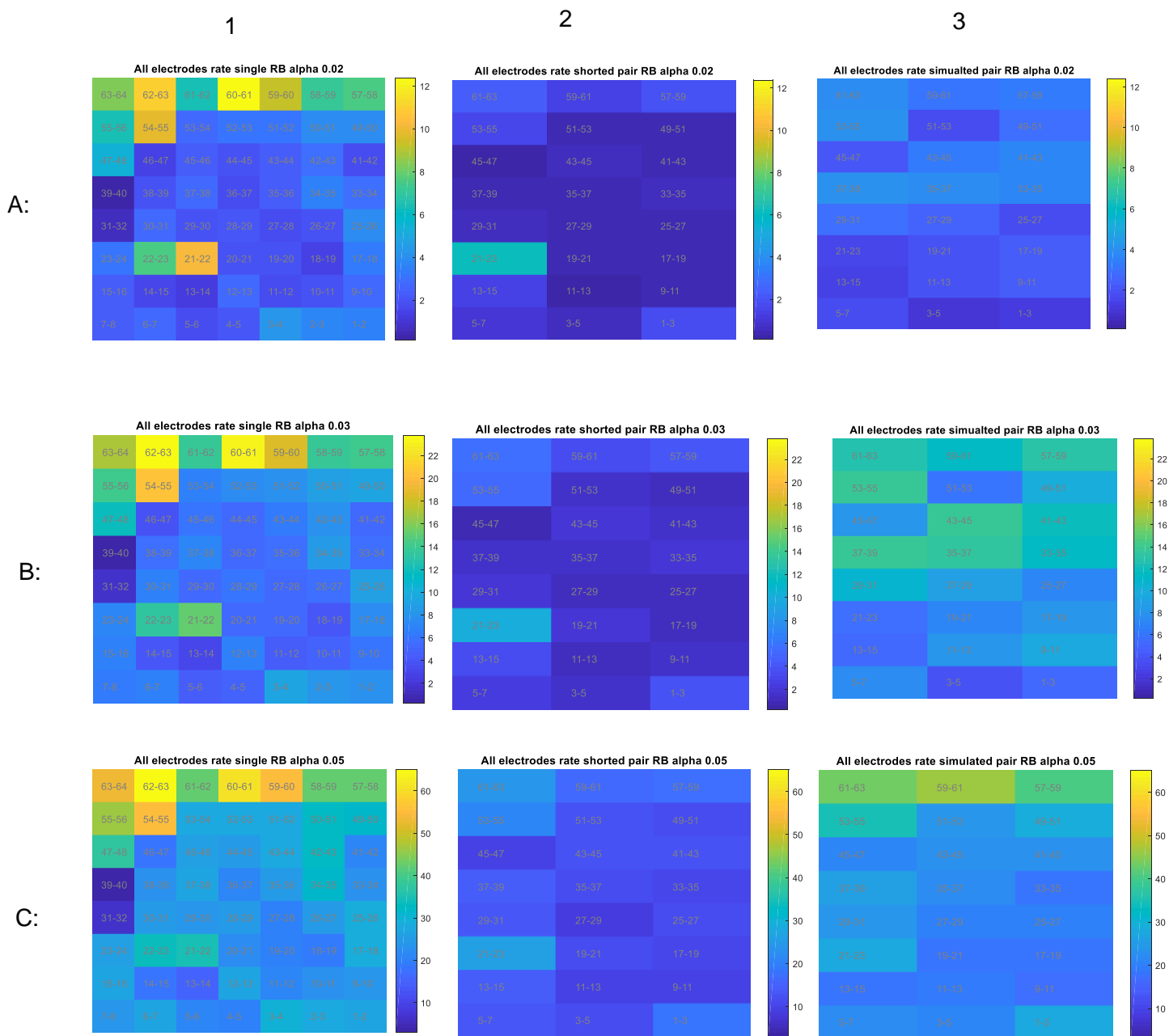


Figure 3.5: Average rate of detected HFOs on the grid in the ripple band. A: Detection with $\alpha = 0.02$. B: Detection with $\alpha = 0.03$. C: Detection with $\alpha = 0.05$. Column number 1 shows the single electrode configuration, column number 2 shows the paired electrode configuration, and column number 3 shows the simulated pair electrode configuration. The spatial pattern of HFOs is consistent in the different configurations, but the number of detected HFOs is lower for the paired and simulated configurations.

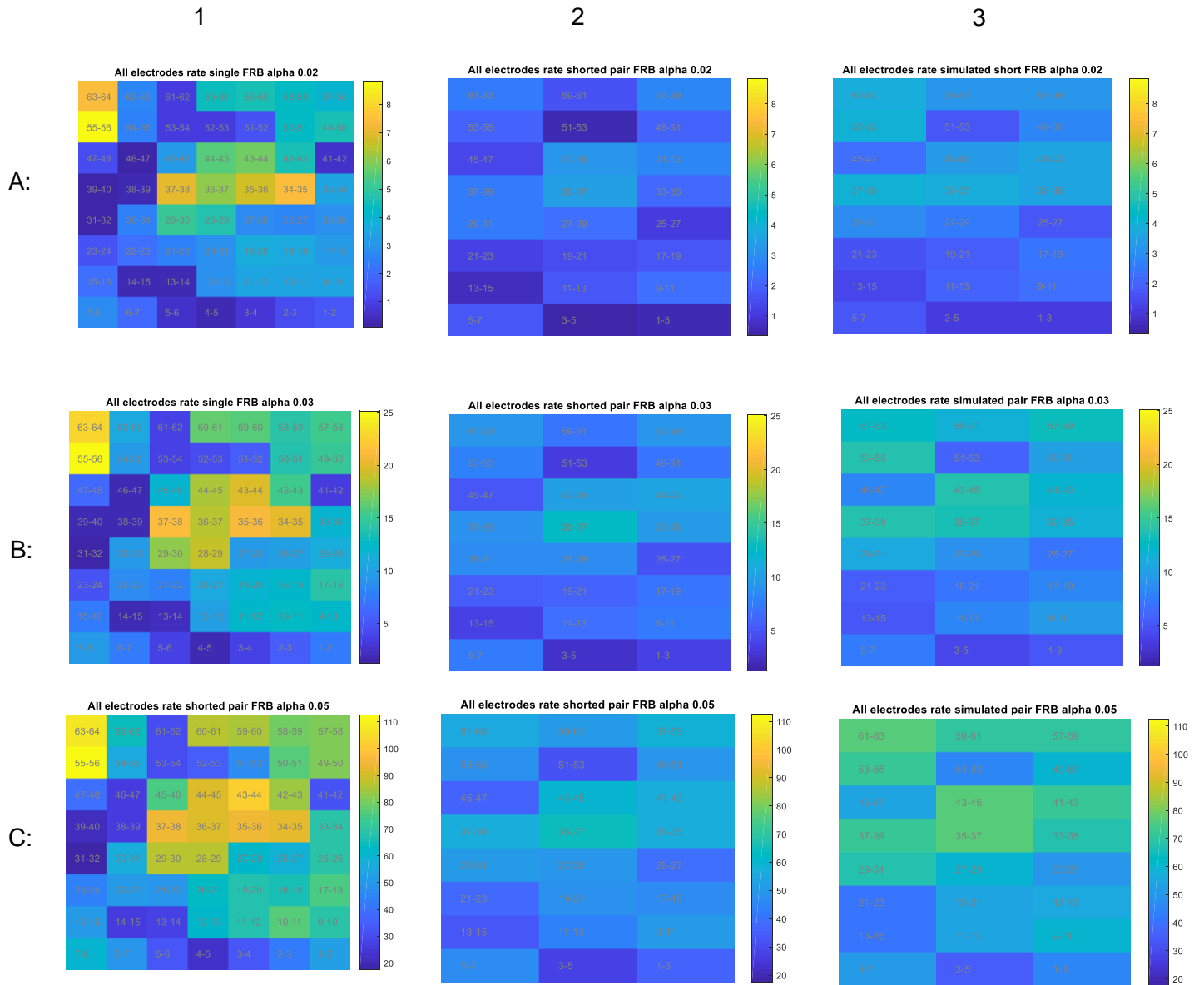


Figure 3.6: Average rate of detected HFOs on the grid in the fast ripple band. A: Detection with $\alpha = 0.02$. B: $\alpha = 0.03$. C: $\alpha = 0.05$. Column number 1 shows the single electrode configuration, Column number 2 shows the paired electrode configuration, and Column number 3 shows the simulated pair electrode configuration. The spatial pattern of HFOs is consistent in the different configurations, but the number of detected HFOs is lower for the paired and simulated paired configurations.

3.4 Statistical testing and comparison

Figures 3.7 and 3.8 illustrate total HFO rate for each one-minute epoch of data used in the statistical analysis. In the bar plots, the total HFO rate per minute is consistent with the results in Figures 3.5 and 3.6. the HFO rate for larger (paired) electrodes is lower than for single electrodes.

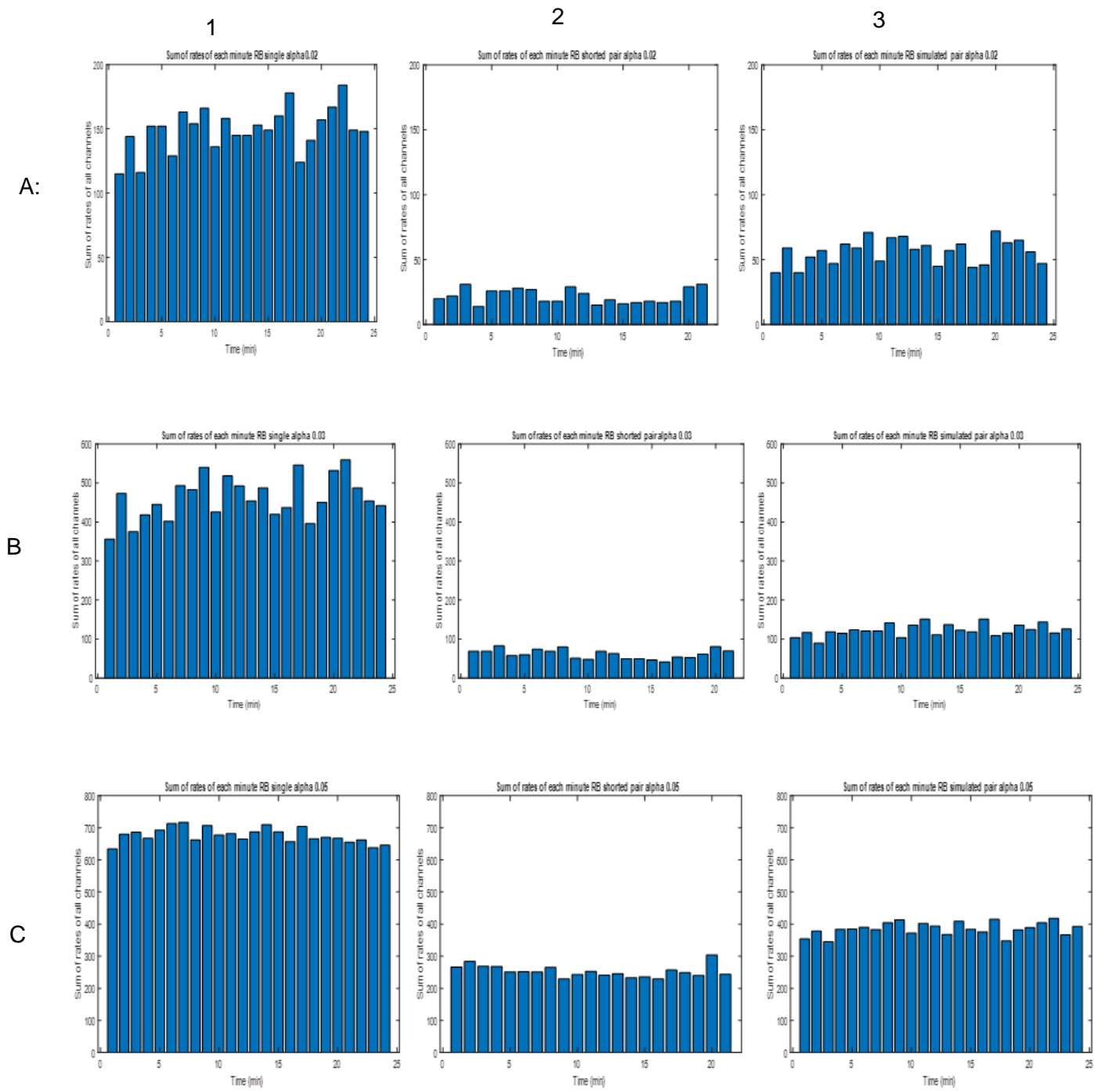


Figure 3.7 : Total HFO rate in the ripple band for each one-minute epoch of data, measured as the sum of rates across all channels. Row A is the results with α value of 0.02. Row B is for α value of 0.03 and Row C is for α value of 0.05. In each row the first column 1: for single electrodes. Column 2 : paired electrodes and column 3 : simulated paired electrodes

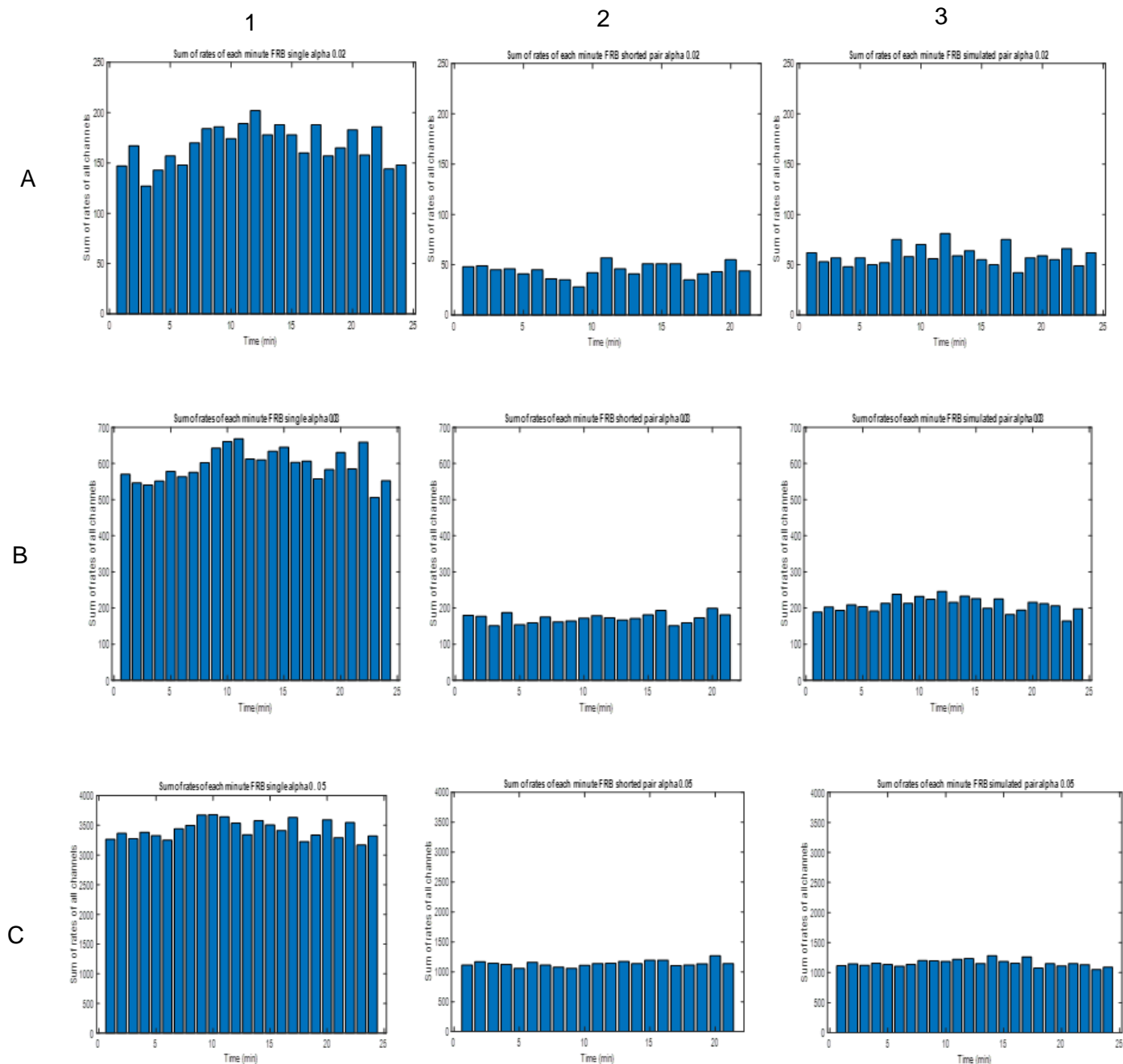


Figure 3.6 : Total HFO rate in the fast ripple band for each one-minute epoch of data, measured as the sum of rates across all channels. Row A is the results with α value of 0.02. Row B is for α value of 0.03 and Row C is for α value of 0.05. In each row the first column 1: for single electrodes. Column 2 : paired electrodes and column 3 : simulated paired electrodes

To compare HFO rates in each configuration, we used the nonparametric Wilcoxon rank sum test, also known as the Mann Whitney U test. We chose this test because the parameters of the distributions of rates in each case were unknown and the number of elements in each distribution was unequal, since the measurements were not conducted for the same amount of time (recordings ranged from 21 to 24 minutes).

In MATLAB, the two-sided Wilcoxon rank sum test tests the null hypothesis that the two independent samples being compared have equal medians. In our analysis, two main comparisons were conducted. First, the total rate of detected HFOs with single electrodes was compared to the case with shorted paired electrodes. Additionally, the rate in the shorted paired electrodes was compared to the simulated shorted electrodes. The comparison between single and paired electrodes demonstrates the difference in the rate of detection with two different sizes of electrodes. The second comparison, between simulated and shorted pairs, compares theoretical mathematical averaging to physical shorting. The statistical tests were repeated for the ripple band and the fast ripple band for three different α values (0.02, 0.03 and 0.05) to test the dependence of the results on the detection threshold. Results of the rank sum test are shown in Table 3.2 and Table 3.2.

Alpha	0.02	0.03	0.05
FRB	p = 2.6430e-07	p = 2.7009e-07	p = 1.0527e-08
RB	p = 1.0319e-08	p = 1.0342e-08	p = 1.0403e-08

Table 3.2: Results of the rank sum test comparing the total HFO rates for the single electrode configuration and the shorted paired configuration.

Alpha	0.02	0.03	0.05
FRB	p = 1.0307e-08	p = 1.0385e-08	p = 1.0469e-08
RB	p = 1.0342e-08	p = 1.0401e-08	p = 1.0480e-08

Table 3.3: Results of the rank sum test comparing the total HFO rates for the shorted paired electrode configuration and the simulated paired configuration.

As the results of the statistical tests show, the null hypothesis of equal medians at the default of $p < 0.05$ was rejected for both comparisons, against the alternative hypothesis of the medians being unequal. In our study, this is interpreted as evidence that the rate of detected HFOs for single electrodes is significantly different than the HFO rate for the shorted paired electrodes. We hypothesize that this is because single electrodes with smaller surface area are detecting smaller events that are not captured by larger contacts. Also, the comparison between the simulated paired configuration and the shorted paired configuration indicates that there is a difference between a physical change in electrode size and mathematical averaging of the electrodes.

Chapter 4 : Discussions and Conclusions

In this study, we designed a novel experimental technique to analyze the impact of electrode size on detection of high frequency oscillations in the brain. The first part of our study consisted of an in vitro experiment using a standard ECoG grid and an agar gel phantom brain. In order to measure the exact same area using electrodes of different sizes, we dynamically changed the surface area of the electrodes by electrically shorting them. This experiment demonstrated the effect of electrode surface area on detection of a simulated signal. We found that the mathematical averages of the signals detected by the individual (unshorted) electrodes were approximately equal to the signals detected by the corresponding shorted electrodes.

However, this experiment had several limitations. The simulated source signal was free of noise and penetrated through the gel material evenly. In the human brain, HFOs can be generated by sources of different sizes, and activity measured by an electrode is the summed combination of many sources. The structure of the brain is also complex, which makes the penetration and spread of the signal more complex than our in vitro experiment. The ECoG grid available to us for this experiment was another limitation. The electrodes used in this experiment were larger than the ones used in our in vivo experiment.

Based on our in vitro experiment, an analogous in vivo experiment was designed. In this case, a smaller HD ECoG grid with 64 channels was implanted

in a patient undergoing evaluation for epilepsy surgery. The HD ECoG grid was placed on the surface of the brain in the location assumed to be the seizure onset zone. The electrodes were shorted together in three different configurations to mimic three different electrode sizes. In our analysis, the difference in the HFO rate suggested that the contact size played a significant role in HFO detection and sheds light on the possibility of different types of HFOs that can each be detected at a different spatial scale. This result is significant because, as opposed to prior studies, our experimental paradigm gave us the means to test different electrode sizes on the exact same brain region. Previously, to study the influence of the contact size, different types of electrodes with different surface areas were recorded simultaneously, but each electrode was implanted in a different part of the brain. We also compared simulated paired electrodes (via mathematical averaging) to the shorted paired electrode configuration. The statistical test in this case indicated that there was a difference between the two groups. We recorded the two configurations at different times, this could be the source of the variation. Also, the noise in the data got worse as more jumpers were added. Therefore, it is possible that the pair recordings contained more false positives.

A major shortcoming of our study was the presence of noise, especially in shorted electrodes. Consequently, we were unable to use the data from the quad electrode configuration that would enable us to test a larger surface area. The power spectrum of our data showed that line noise of 60 Hz and its harmonics were the most dominant type of noise. As we were interested in the frequency range of 80-500Hz, we were unable to exclude the data that contained harmonics

of higher frequencies. We believe that the addition of the jumpers to the t-connector created a large antenna, which captured noise from all directions. To help mitigate this, we disconnected and turned off all electronic devices in the room (except those that were critical for patient care). This helped, but did not solve the problem. Therefore, for future experiments, we propose to place the T-connector in a faraday cage (Figure 4.1). The Faraday cage will block the electromagnetic fields created by electronic devices present in the room and will reduce the amplitude of 60 Hz line noise and its harmonics in our data.

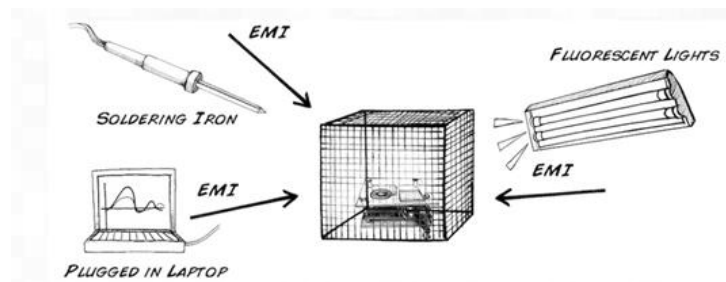


Figure 4.1: Faraday cage to block the EMF present in the environment.

Another limitation of the in vivo study was that the electrode connections for the quad configuration were not the same format as our mathematical model. They were accidentally connected in a 1x4 configuration instead of a 2x2 configuration. This would have complicated the comparison between the in vivo and in vitro results; however, due to the presence of noise in the recordings, we decided not to analyze this configuration anyway. For future studies, the electrode shorting configuration will be the same as the in vitro study and the mathematical model.

To have a more comprehensive conclusion, more participants will also need to be recruited. However, the results presented here include a theoretical model of the effect of electrode size on HFO amplitude, validation in an in vitro experiment with a phantom brain, and proof-of-concept recordings in one human subject.

In conclusion, our experimental studies found that detection of HFOs is impacted by electrode size, with smaller electrodes able to detect more HFOs. The difference in the rate of detection verifies our hypothesis. As HFOs gain traction as a clinical biomarker for seizure onset zone localization, understanding the properties of HFOs more comprehensively is crucial.

In the long term, this work can also enlighten our knowledge of the size of the underlying neuronal generators, as well as optimal parameters and electrode size in HFO recording. These results can be applied in clinical routine to improve SOZ localization and surgical outcome.

References:

- 1 - Kucewicz M.T., et al., *High frequency oscillations are associated with cognitive processing in human recognition memory*. Brain, 2014. 137(Pt 8): p. 2231-44.
- 2- Lachaux J.P., et al., *High-frequency neural activity and human cognition: past, present and possible future of intracranial EEG research*. Prog Neurobiol, 2012. 98(3): p. 279-301.
- 3 - Matsumoto A., et al., *Pathological and physiological high-frequency oscillations in focal human epilepsy*. J Neurophysiol, 2013. 110(8): p. 1958-64.
- 4 - Bragin A., et al., *High-frequency oscillations in epileptic brain*. Curr Opin Neurol. 2010;23(2):151–156. doi:10.1097/WCO.0b013e3283373ac8
- 5 - IOM (Institute of Medicine), *Epilepsy Across the Spectrum: Promoting Health and Understanding* 2012, Washington, D.C.: The National Academies Press.
- 6 - Jacobs J., et al., *High-frequency oscillations (HFOs) in clinical epilepsy*. Prog Neurobiol, 2012. 98(3): p. 302-15.
- 7 - Zijlmans M., et al., *High-frequency oscillations as a new biomarker in epilepsy*. Ann Neurol, 2012. 71(2): p. 169-78.
- 8 - Fujiwara, H., et al., *Resection of ictal high frequency oscillations is associated with favorable surgical outcome in pediatric drug resistant epilepsy secondary to tuberous sclerosis complex*. Epilepsy Res, 2016. 126: p. 90-7.
- 9 - Fedele, T., et al., *Automatic detection of high frequency oscillations during epilepsy surgery predicts seizure outcome*. Clin Neurophysiol, 2016. 127(9): p. 3066-74.
- 10 - Yazdanpour-Naeini,R., *Automatic detection of high frequency oscillations of neural signals in epileptic patients*. Diss. Concordia University, 2012.
- 11 - Zijlmans M., et al., *High frequency electroencephalographic oscillations correlate with outcome of epilepsy surgery*. Ann Neurol 2010; 67:209–220.
- 12 - Jacobs J, et al., (2012). *High-frequency oscillations (HFOs) in clinical epilepsy*. Prog. Neurobiol. 98, 302–315.
- 13 - Jacobs J, et al., *Interictal high-frequency oscillations (80-500 Hz) are an indicator of seizure onset areas independent of spikes in the human epileptic brain*. Epilepsia, 2008. 49(11): p. 1893-907.

- 14 - Bragin A., et al., *High-frequency oscillations after status epilepticus: epileptogenesis and seizure genesis*. *Epilepsia*, 2004. 45(9): p. 1017-23.
- 15- Worrell G.A., et al., *High-frequency oscillations in human temporal lobe: simultaneous microwire and clinical macroelectrode recordings*. *Brain*, 2008. 131(Pt 4): p. 928-37.
- 16-. Jacobs J., et al., *Value of electrical stimulation and high frequency oscillations (80-500 Hz) in identifying epileptogenic areas during intracranial EEG recordings*. *Epilepsia*, 2010. 51(4): p. 573-82.
- 17 -. Pail M., et al., *Intracerebrally recorded high frequency oscillations: simple visual assessment versus automated detection*. *Clin Neurophysiol*, 2013. 124(10): p. 1935-42.
- 18 - Akiyama T., et al., *Focal resection of fast ripples on extraoperative intracranial EEG improves seizure outcome in pediatric epilepsy*. *Epilepsia*, 2011. 52(10): p. 1802-11.
- 19 - Urrestarazu E., et al., *Interictal high-frequency oscillations (100-500 Hz) in the intracerebral EEG of epileptic patients*. *Brain*, 2007. 130(Pt 9): p. 2354-66.
- 20 - Pail M., et al., *Intracerebrally recorded high frequency oscillations: simple visual assessment versus automated detection*. *Clin Neurophysiol*, 2013. 124(10): p. 1935-42.
- 21 - Burnos S., et al., *Human intracranial high frequency oscillations (HFOs) detected by automatic time-frequency analysis*. *PLoS One*, 2014. 9(4): p. e94381.
- 22 - Kerber K., et al., *Differentiation of specific ripple patterns helps to identify epileptogenic areas for surgical procedures*. *Clin Neurophysiol*, 2013.
- 23 - von Ellenrieder N., et al., *Automatic detection of fast oscillations (40-200 Hz) in scalp EEG recordings*. *Clin Neurophysiol*, 2012. 123(4): p. 670-80.
- 24 - Melani F., et al., *Occurrence of scalp-fast oscillations among patients with different spiking rate and their role as epileptogenicity marker*. *Epilepsy Res*, 2013. 106(3): p. 345-56.
- 25 - Pearce A., et al., *Temporal changes of neocortical high-frequency oscillations in epilepsy*. *J Neurophysiol*, 2013. 110(5): p. 1167-79.
- 26 - Kobayashi K., et al., *Very fast rhythmic activity on scalp EEG associated with epileptic spasms*. *Epilepsia*, 2004. 45(5): p. 488-496.
- 27 - Okanishi T., et al., *Interictal high frequency oscillations correlating with seizure outcome in patients with widespread epileptic networks in tuberous sclerosis complex*. *Epilepsia*, 2014. 55(10): p. 1602-10.
- 28 - von Ellenrieder N., et al., *Size of cortical generators of epileptic interictal events and visibility on scalp EEG*. *Neuroimage*, 2014. 94: p. 47-54.

- 29 - Chatillon C.E., et al., *Influence of contact size on the detection of HFOs in human intracerebral EEG recordings*. Clin Neurophysiol, 2013. 124(8): p. 1541-6.
- 30 - Burnos S., et al., *Human intracranial high frequency oscillations (HFOs) detected by automatic time-frequency analysis*. PLoS One, 2014. 9(4): p. e94381.
- 31 - Kerber K., et al., *Differentiation of specific ripple patterns helps to identify epileptogenic areas for surgical procedures*. Clin Neurophysiol, 2013.
- 32 - Schevon C.A., et al., *Spatial characterization of interictal high frequency oscillations in epileptic neocortex*. Brain, 2009. 132(Pt 11): p. 3047-59.
- 33 - Staba R.J., et al., *Quantitative analysis of high-frequency oscillations (80-500 Hz) recorded in human epileptic hippocampus and entorhinal cortex*. J Neurophysiol, 2002. 88(4): p. 1743-52.
- 34 - Zelman R., et al., *Scalp EEG is not a blur: it can see high frequency oscillations although their generators are small*. Brain Topogr, 2014. 27(5): p. 683-704.
- 35 - Kobayashi K., et al., *A storm of fast (40-150Hz) oscillations during hypsarrhythmia in West syndrome*. Ann Neurol, 2015. 77(1): p. 58-67.
- 36 - Kobayashi K., et al., *High-frequency oscillations in idiopathic partial epilepsy of childhood*. Epilepsia, 2011. 52(10): p. 1812-9.
- 37 - Worrell GA., et al. *High-frequency oscillations in human temporal lobe: simultaneous microwire and clinical macroelectrode recordings*. Brain. 2008;131:928–37.
- 38 – Menendez de la Prida L., et al., *Conundrums of high-frequency oscillations (80-800 Hz) in the epileptic brain*. J Clin Neurophysiol. 2015;32(3):207–219.
- 39 - Nelson, M.J., et al., *Review of signal distortion through metal microelectrode recording circuits and filters*. J Neurosci Methods, 2008. 169(1): p. 141-57.
- 40 - Robinson, D.A., *The electrical properties of metal microelectrodes*. Proceedings of the IEEE, 1968. 56(6).
- 41 - Bragin A, et al., *Ripples and fast ripples in the human epileptic brain. Depth profiles and unit correlates*. Epilepsia. 2000;41:8
- 42 – Charupanit K, et al., *A Simple Statistical Method for Automated Detection of Ripples in Human Intracranial EEG*. Brain Topography. 2017; 30(6):724-738.